# Search for the ground-state electronic configurations of correlated organometallic metallocenes from constraint density functional theory

Kenji Nawa,[1,*] Yukie Kitaoka,[2] Kohji Nakamura,[1,†] Hiroshi Imamura,[2] Toru Akiyama,[1] Tomonori Ito,[1] and M. Weinert[3,‡]

[1]*Department of Physics Engineering, Mie University, Tsu, Mie 514-8507, Japan*

[2]*National Institute of Advanced Industrial Science and Technology (AIST), Spintronics Research Center, Tsukuba, Ibaraki 305-8568, Japan*

[3]*Department of Physics, University of Wisconsin-Milwaukee, Milwaukee, Wisconsin 53201, USA*

(Received 18 February 2016; revised manuscript received 21 June 2016; published 18 July 2016)

The ground-state electronic configurations of the correlated organometallic metallocenes, $M\mathrm{Cp}_2$, $M$ = V, Cr, Mn, Fe, Co, and Ni, are investigated using constraint density functional theory combined with nonempirical $U_{\mathrm{eff}}$ parameters determined from linear-response theory. The relative stability of the various $d$-orbital electronic configurations of these organometallic molecules is found to be sensitive to the amount of correlation. Using nonempirical values of $U_{\mathrm{eff}}$, the calculated electronic configurations are in agreement with the experiments: ${}^4A_{2g}$, ${}^3E_{2g}$, ${}^6A_{1g}$, ${}^1A_{1g}$, ${}^2E_{1g}$, and ${}^3A_{2g}$ for the $\mathrm{VCp}_2$, $\mathrm{CrCp}_2$, $\mathrm{MnCp}_2$, $\mathrm{FeCp}_2$, $\mathrm{CoCp}_2$, and $\mathrm{NiCp}_2$, respectively.

DOI: 10.1103/PhysRevB.94.035136

## I. INTRODUCTION

Organometallic molecules are increasingly finding use in novel applications because their electronic and magnetic properties can be tuned by varying metal elements [1–5]. For organometallic molecules where the electronic configurations of $d(f)$ electrons are an essential aspect, the complexity of the orbital degeneracy and the changes due to the presence of the ligand field of molecules complicate the theoretical analysis of even the ground state with the consequence that *ab initio* calculations based on the density functional theory (DFT) often fail to obtain the experimentally observed ground-state electronic configuration.

This difficulty is intrinsically related to the fact that the various electronic configurations belonging to different irreducible representations are all compatible with the symmetry of the charge (and spin) density (completely symmetric representation), i.e., the *symmetry* of the charge density is not sufficient to distinguish among the electronic configurations. Moreover, correlation effects for organometallic molecules may become important [6,7], further complicating the analysis; for example, the calculations may be trapped in one of the multiple local minima corresponding to the various electronic configurations. Thus, searching for the ground-state electronic configuration in correlated systems using DFT remains a significant challenge.

In order to overcome such difficulties, constraint DFT provides a powerful tool for exploring the low-energy electronic configurations compatible with a given ligand symmetry. Here, we apply constraint DFT systematically to the prototypical organometallic molecules, metallocenes $M\mathrm{Cp}_2$ [8,9] for the $3d$ transition metals ($M$'s) from V to Ni. The calculations use the full-potential linearized augmented plane-wave (FLAPW) method [10,11] including on-site Coulomb interaction corrections $+U$ [12]. As shown previously [13,14], constraint DFT is a viable approach to search for the ground-state $d$-orbital electronic configuration in systems where correlation effects play an important role. Here we demonstrate that this approach—combined with nonempirical values of $U$—is also capable of obtaining agreement with experiments for the correlated organometallic molecules with their high degree of electronic complexity.

## II. MODEL AND METHOD

The atomic structure of the $M\mathrm{Cp}_2$ molecules with the two fivefold cyclopentadienyl rings $\mathrm{Cp}_2$ is shown in Fig. 1(a); a schematic energy-level diagram in the crystal field is given in Fig. 1(b). Both eclipsed and staggered conformations exist; here we focus on the latter, which has been the reported structure in a number of experiments [15–18]. The metal atom at the center of the molecule between the two Cp rings sits at a site of $D_{5d}$ symmetry such that the $d$ orbitals are split into three states: a singlet $d_{z^2}$ and two doublets $d_{xz,yz}$,$d_{x^2-y^2,xy}$. The $d_{xz,yz}$ state may be further pushed up in energy due to the hybridization with the $\mathrm{Cp}_2$ $e_{1g}$ orbital, whereas the $d_{x^2-y^2,xy}$ state goes down due to the hybridization with the $e_{2g}$ orbital as illustrated in Figs. 1(c) and 1(d), respectively. The $d_{z^2}$ state with no direct overlap to the molecular orbitals may have the lowest energy of the $d$ states.

The experimentally reported ground-state electronic configurations [15–18] are summarized in Table I. Photoelectron spectroscopy measurements of $\mathrm{FeCp}_2$ in the gas phase reveal a $S = 1$ spin multiplet corresponding to orbital occupations of the ${}^1A_{1g}$ state ($d^2_{z^2}$,$d^4_{x^2-y^2,xy}$) [15,16]. For $\mathrm{VCp}_2$, $\mathrm{CrCp}_2$, $\mathrm{MnCp}_2$, $\mathrm{CoCp}_2$, and $\mathrm{NiCp}_2$ in gas phases, ${}^4A_{2g}$, ($d^1_{z^2}$,$d^2_{x^2-y^2,xy}$), ${}^3E_{2g}$ ($d^1_{z^2}$,$d^3_{x^2-y^2,xy}$), ${}^6A_{1g}$($d^1_{z^2}$, $d^2_{x^2-y^2,xy}$,$d^2_{xz,yz}$), ${}^2E_{1g}$ ($d^2_{z^2}$,$d^4_{x^2-y^2,xy}$,$d^1_{xz,yz}$), and ${}^3A_{2g}$ ($d^2_{z^2}$, $d^4_{x^2-y^2,xy}$,$d^2_{xz,yz}$) were systematically observed [15,16] where the spin multiplicity $S$ decreases from $\mathrm{VCp}_2$ ($S = 4$) to $\mathrm{FeCp}_2$ (1), except for $\mathrm{MnCp}_2$ (6), and then it increases in $\mathrm{CoCp}_2$ (2) and $\mathrm{NiCp}_2$ (3). A high-spin state ${}^6A_{1g}$ of $\mathrm{MnCp}_2$ was further identified by electron spectroscopy and nuclear magnetic resonance measurements [17,18]. However, the DFT ground states are still a matter of debate due to the complexity and difficulty of incorporating correlation effects. For example, for $\mathrm{MnCp}_2$, $+U$ calculations predict the low-spin ${}^2E_{2g}$ state [19] whereas hybrid functional B3LYP calculations predict the high-spin ${}^6A_{1g}$ state [20]. Furthermore, both calculations

*nawa12@nd.phen.mie-u.ac.jp
†kohji@phen.mie-u.ac.jp
‡weinert@uwm.edu

 ©2016 American Physical Society

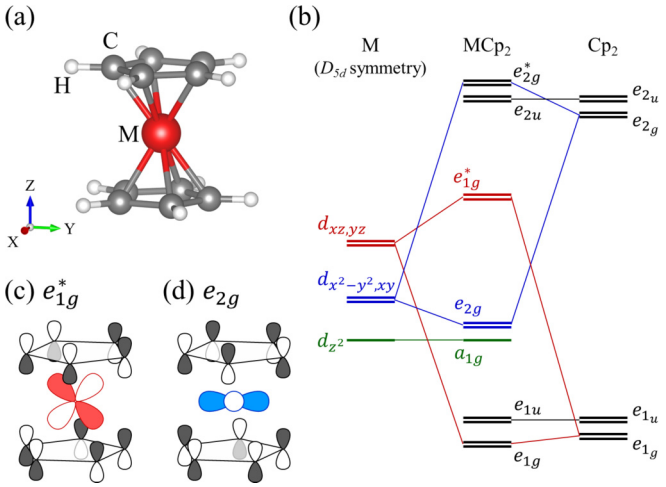


FIG. 1. (a) Structure of a metallocene where large (red), middle (gray), and small (white) circles indicate transition-metal, carbon, and hydrogen atoms, respectively. (b) Schematic of the energy diagrams of the crystal-field splitting of transition-metal ($M$) $d$ orbitals for $D_{5d}$ symmetry, the molecular orbitals in the two cyclopentadienyl rings $Cp_2$, and the hybridized orbitals in the $MCp_2$. (c) and (d) Schematics of the molecular $e^*_{1g}$ (antibonding $M$ $d_{xz,yz}$-$Cp_2$ $e_{1g}$) and $e_{2g}$ (bonding $M$ $d_{x^2-y^2,xy}$-$Cp_2$ $e_{2g}$) states in $MCp_2$.

for $CrCp_2$ ($^3A_{1g}$) disagree with the ($^3E_{2g}$) state found by experiment.

To model the isolated $MCp_2$, a slab with infinite vacuum on both sides was adopted with a large in-plane lattice constant of 18 a.u. Calculations were carried out by using the film-FLAPW [10,11] method based on the GGA [21] with $+U$ [12]. A cutoff of $|\mathbf{k}+\mathbf{G}| \leqslant 3.6$ a.u.$^{-1}$ was used to expand the wave functions. The muffin-tin radii and lattice harmonic expansions for the charge and spin densities were 2.2 a.u., $\ell = 8$; 1.1 a.u., $\ell = 6$; and 0.8 a.u., $\ell = 4$ for the $M$, C, and H atoms, respectively. Atomic positions were fully optimized.

TABLE I. Ground-state electronic configurations in the present constraint DFT calculations for both generalized gradient approximation (GGA) and GGA + $U$, compared to previous GGA + $U$ ($U_{\text{eff}}$ of 3.0 eV) [19], hybrid functional Becke three-parameter Lee-Yang-Parr (B3LYP) [20] calculations, and experiments [15–18] for $MCp_2$ ($M$ = V, Cr, Mn, Fe, Co, and Ni). The $U_{\text{eff}}$ (in eV) in the parentheses of the third column are determined from constraint DFT calculations based on the linear-response theory (LRT).

| | Present calculations | | Previous calculations | | |
|---|---|---|---|---|---|
| | GGA | GGA + $U$ ($U_{\text{eff}}$) | GGA + $U$ | B3LYP | Experiments |
| V | $^4A_{2g}$ | $^4A_{2g}$ (2.3) | $^4A_{1g}$[a] | $^4A_{1g}$[a] | $^4A_{2g}$ |
| Cr | $^3E_{2g}$ | $^3E_{2g}$ (2.3) | $^3A_{1g}$ | $^3A_{1g}$ | $^3E_{2g}$ |
| Mn | $^2E_{2g}$ | $^6A_{1g}$ (2.4) | $^2E_{2g}$ | $^6A_{1g}$ | $^6A_{1g}$ |
| Fe | $^1A_{1g}$ | $^1A_{1g}$ (2.5) | $^1A_{1g}$ | $^1A_{1g}$ | $^1A_{1g}$ |
| Co | $^2E_{1g}$ | $^2E_{1g}$ (2.6) | $^2E_{1g}$ | $^2E_{1g}$ | $^2E_{1g}$ |
| Ni | $^3A_{2g}$ | $^3A_{2g}$ (2.4) | $^3A_{2g}$ | $^3A_{2g}$ | $^3A_{2g}$ |

[a]The electronic configuration in Refs. [15–18] is identical to that of $^4A_{2g}$.

The energy functional in constraint DFT for a given electronic configuration and site symmetry is given by

$$E\left[\rho(\mathbf{r}), n^{\alpha}_{mm'}\right] = E_{\text{GGA}}[\rho(\mathbf{r})] + \left[E_{ee}\left(n^{\alpha}_{mm'}\right) - E_{dc}(n^{\alpha})\right] + \sum_{mm'} \mu^{\alpha}_{m'm}\left(n^{\alpha}_{mm'} - N^{\alpha}_{mm'}\right). \quad (1)$$

The first term is the standard total energy functional in the GGA. The second term is the on-site correlation correction $+U$, introduced using the rotational invariant formula [12], where $E_{ee}$ and $E_{dc}$ are the electron-electron interaction energy and double counting terms, respectively, and both are functions of the $d$-orbital density matrix $n^{\alpha}_{mm'}$ ($n^{\alpha} = \sum_m n^{\alpha}_{mm}$) at an atomic site $\alpha$. The third term constrains the occupation numbers $n^{\alpha}_{mm'}$ for a given electronic configuration, where $N^{\alpha}_{mm'}$ is the desired value and $\mu^{\alpha}_{m'm}$ is the corresponding constraint field (Lagrange multiplier). When all the $\mu^{\alpha}_{m'm}$'s are zero, the solution is the same as for the GGA + $U$ functional.

By the variational principle, the Kohn-Sham equations corresponding to Eq. (1) are

$$\left[H_{\text{GGA}} + \sum_{m'm}\left(V^{\sigma}_{m'm} + \mu^{\alpha}_{m'm}\right)\hat{P}^{\alpha}_{mm'}\right]\Phi_b = \epsilon\Phi_b, \quad (2)$$

where $V^{\sigma}_{m'm}$ is the effective on-site Coulomb interaction matrix. In the LAPW basis, the projection operator $\hat{P}^{\alpha}_{mm'}$ onto the $mm'$ subspace is given by

$$\hat{P}^{\alpha}_{mm'} = \left|u^{\alpha}_l Y_{lm}\right\rangle\left\langle u^{\alpha}_l Y_{lm'}\right| + \frac{1}{\langle \dot{u}_l \dot{u}_l\rangle}\left|\dot{u}^{\alpha}_l Y_{lm}\right\rangle\left\langle \dot{u}^{\alpha}_l Y_{lm'}\right|, \quad (3)$$

and $n^{\alpha}_{mm'}$ is

$$n^{\alpha}_{mm'} = \sum_b f_b \langle\Phi_b|\hat{P}^{\alpha}_{mm'}|\Phi_b\rangle. \quad (4)$$

In practice, we specify a set of constraint fields $\mu^{\alpha}_n$ along the directions of the eigenvectors of $n^{\alpha}_{mm'}$ consistent with the site symmetry. Then, the $\mu^{\alpha}_{m'm}$, which are rotated back from the $\mu^{\alpha}_n$, are introduced in Eq. (2), and the corresponding $n^{\alpha}_{mm'}$ are determined self-consistently. The total energy is calculated using Eq. (1) with $N^{\alpha}_{mm'} = n^{\alpha}_{mm'}$.

In contrast to standard practice where the effective Coulomb parameter $U^{\alpha}_{\text{eff}} = U^{\alpha} - J^{\alpha}$ is implicitly a model parameter often chosen to match experiment for some system, we evaluate it for each molecule based on LRT [22]: $U^{\text{LRT},\alpha}_{\text{eff}}$ was estimated from the interacting ($\chi$) and noninteracting ($\chi_0$) response matrices as

$$U^{\text{LRT},\alpha}_{\text{eff}} = \left(\chi_0^{-1} - \chi^{-1}\right)_{\alpha\alpha}. \quad (5)$$

The response matrices are the variations of orbital occupation at site $\beta$,

$$\chi_{\beta\alpha} = \frac{\partial n^{\beta}}{\partial \mu^{\alpha}}, \quad \chi_{0\beta\alpha} = \frac{\partial n^{\beta}_0}{\partial \mu^{\alpha}}, \quad (6)$$

when a constraint $\mu^{\alpha}$, a small external potential, at site $\alpha$ is introduced. The derivatives were numerically computed by using the constraint DFT approach, i.e., Eq. (1) without the $+U$ terms, where $\chi_0$ is obtained at the first iteration of the self-consistent cycle starting from the self-consistent unconstrained system [22].

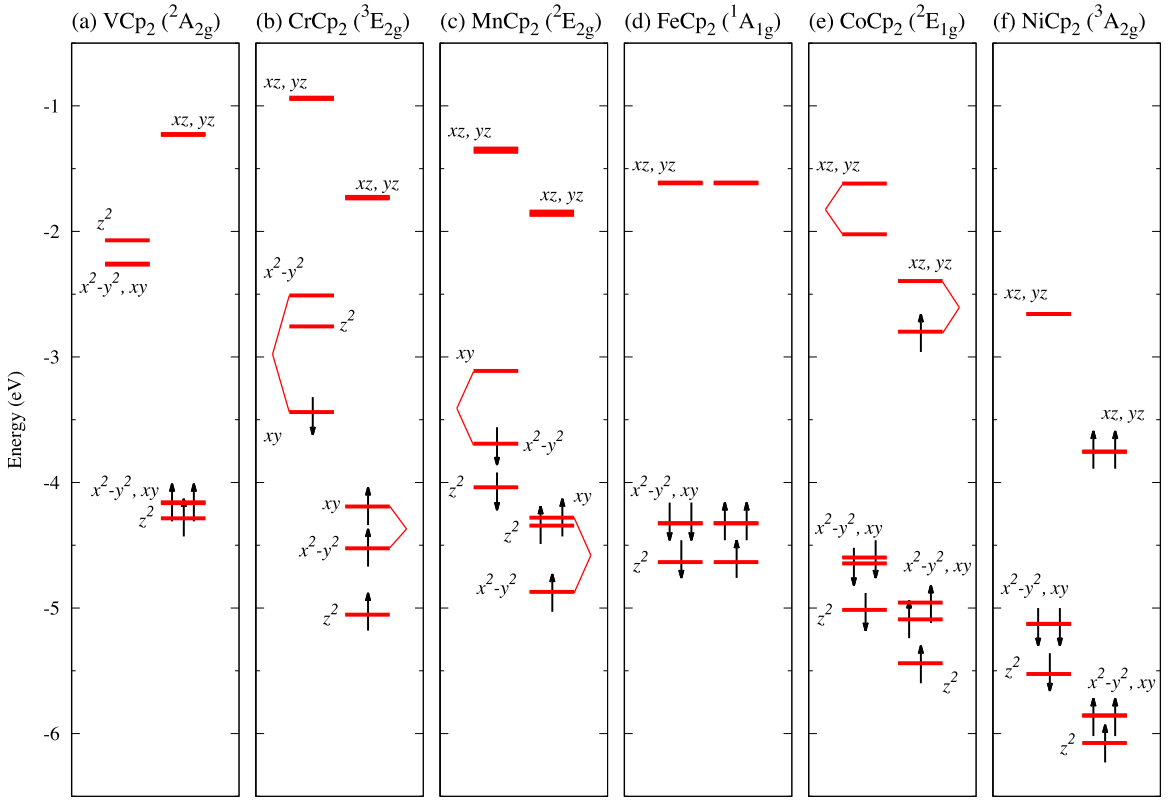


FIG. 2. Energy diagram of the $d$ orbitals in (a) $VCp_2$ ($^4A_{2g}$), (b) $CrCp_2$ ($^3E_{2g}$), (c) $MnCp_2$ ($^2E_{2g}$), (d) $FeCp_2$ ($^1A_{1g}$), (e) $CoCp_2$ ($^2E_{1g}$), and (f) $NiCp_2$ ($^3A_{2g}$), calculated using GGA. Up and down arrows indicate the electron occupations of the majority- and minority-spin states, respectively. The reference energy (0 eV) is set to the vacuum level.

## III. RESULTS AND DISCUSSION

Figures 2 and 3 summarize the energy positions of the $d$ orbitals in the ground-state electronic configurations for $MCp_2$ ($M$ = V, Cr, Mn, Fe, Co, and Ni) for both the GGA ($U_{\text{eff}} = 0$ eV) and the GGA + $U$. These electronic configurations were determined by changing the set of constraint fields $\mu_n^\alpha$ as demonstrated previously [13,14] with the values of $U_{\text{eff}}^{\text{LRT}}$ obtained using Eq. (5) from the structures geometrically optimized within the GGA; the values of $U_{\text{eff}}^{\text{LRT}}$ are almost the same for all molecules, varying between 2.3 and 2.6 eV.

First, we consider $FeCp_2$. There is no change in the ground state in the GGA + $U$ compared to the GGA: The $d_{x^2-y^2,xy}$ and $d_{z^2}$ states are fully occupied, and a large energy gap of 2.8 eV appears between the highest occupied and lowest unoccupied states, forming a closed shell with $^1A_{1g}$ symmetry. No stationary solutions of the other electronic configurations were observed in the constraint DFT calculations, even for large constraint fields $\mu_n$ up to 10 eV. Thus, the electronic configuration of the $^1A_{1g}$ state is energetically the most stable as expected from the "18-electron rule" [23] describing stable metal complexes.

For $CoCp_2$ and $NiCp_2$ since the number of electrons is larger than that of $FeCp_2$, the doublet $d_{xz,yz}$ is occupied by a single electron for $CoCp_2$ and by two electrons for $NiCp_2$, leading to $^2E_{1g}$ and $^3A_{2g}$ ground states, respectively. In both molecules, no stationary solutions of the other electronic configurations exist in either the GGA or the GGA + $U$, and the inclusion of $U$ does not change the ground state. Calculations confirm that for the $^2E_{1g}$ state of $CoCp_2$, the degeneracy in the doublet $d_{xz,yz}$ occupied by a single electron is removed by a Jahn-Teller distortion that lowers the site symmetry to $C_{2h}$. The predicted ground states of both $CoCp_2$ and $NiCp_2$ agree with experiments [15–18].

Interestingly, for $MnCp_2$ where the number of electrons is smaller than in $FeCp_2$, two stationary solutions of the low-spin and the high-spin $^6A_{1g}$ states are observed. In the GGA, the calculated total energy indicates the ground state is $^2E_{2g}$ with the $^6A_{1g}$ state higher in energy by 0.77 eV. However, the electron correlations ($+U$) change the ground state to the $^6A_{1g}$ state, in agreement with experiments. This result is in contrast to the previous $+U$ calculations where the $^2E_{2g}$ state was predicted [19].

We further find that for $MnCp_2$ the total energies of the $^6A_{1g}$ and $^2E_{2g}$ states at $U_{\text{eff}} = 2$ eV are nearly degenerate. Figure 4(a) shows the relative energy $\Delta E$ of the two states as a function of $U_{\text{eff}}$ where the molecular structures were fully optimized at each $U_{\text{eff}}$. When $U_{\text{eff}}$ increases, $\Delta E$ of the $^6A_{1g}$ configuration monotonically decreases and becomes stable for $U_{\text{eff}}$ greater than $\sim$2 eV. The present constraint DFT calculations employing the nonempirical $U_{\text{eff}}^{\text{LRT}}$ (=2.4 eV) from the linear-response theory thus reproduce experiments [15–18]. Importantly, starting the self-consistent calculations with no constraints naturally yields the $^2E_{2g}$ solution; thus, in this case constraint DFT is essential in the search for the true ground state.

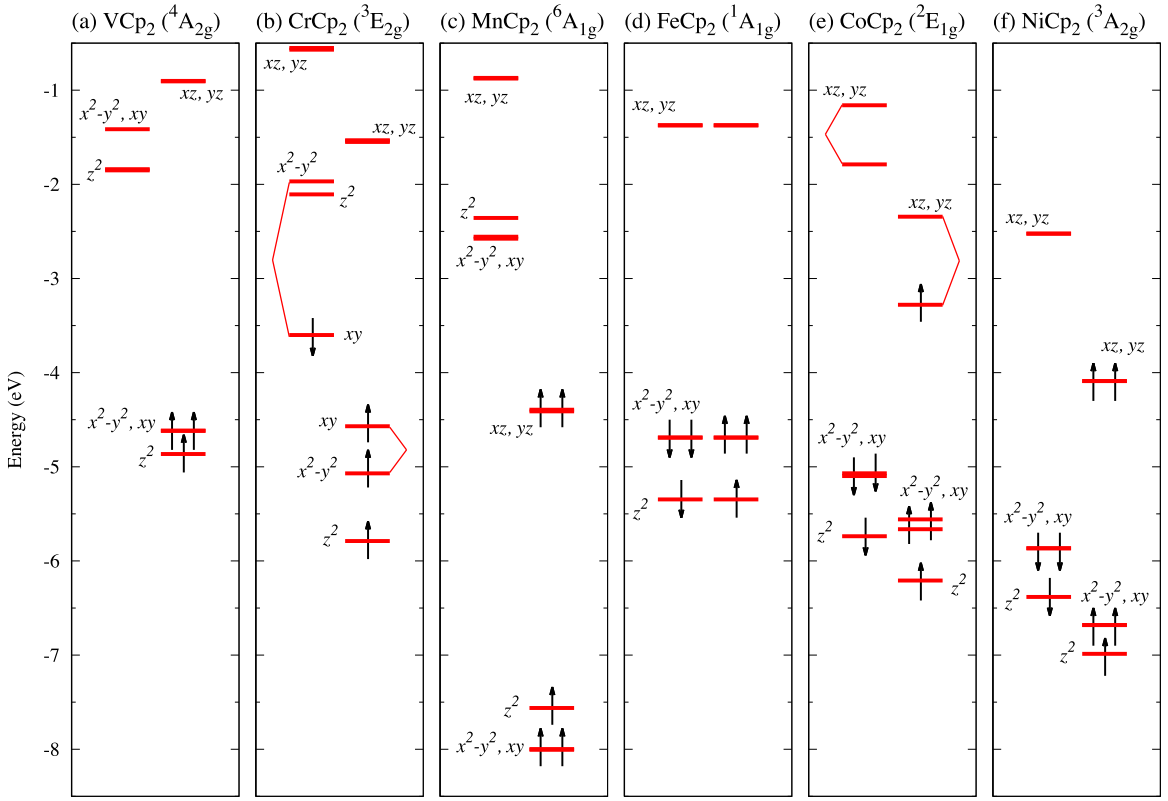


FIG. 3. Energy diagram of the $d$ orbitals in (a) $VCp_2$ ($^4A_{2g}$), (b) $CrCp_2$ ($^3E_{2g}$), (c) $MnCp_2$ ($^6A_{1g}$), (d) $FeCp_2$ ($^1A_{1g}$), (e) $CoCp_2$ ($^2E_{1g}$), and (f) $NiCp_2$ ($^3A_{2g}$), calculated using the GGA + $U$ with the $U_{\rm eff}^{\rm LRT}$ values in Table I. Notation is the same as in Fig. 2.

Note that the $^2E_{2g}$ state could in principle be stabilized by the Jahn-Teller effect, i.e., a lifting of the degeneracy of the doublet $d_{x^2-y^2,xy}$ in the minority-spin states. However, the $^6A_{1g}$ state—with fully occupied majority-spin states and empty minority-spin states—is still favorable due to the large exchange splitting arising from the electron correlation ($+U$) effects. Thus, the high-spin electronic configuration with $S = 5/2\mu_{\rm B}$ is preferable as expected by Hund's first rule. As shown in Fig. 5(a), the charge-density difference

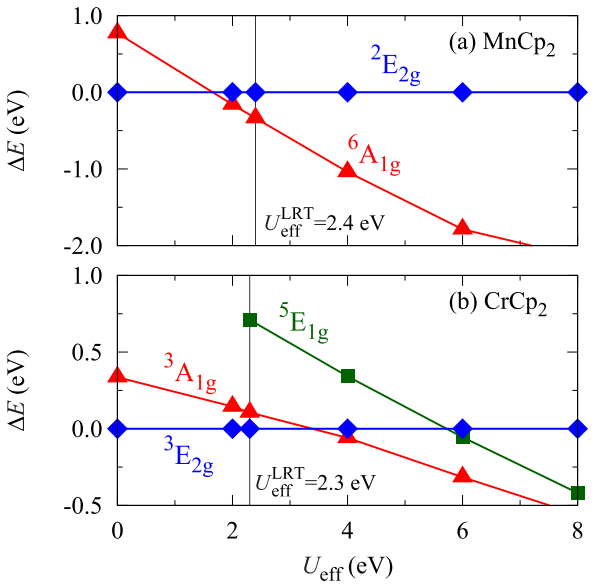


FIG. 4. Total energy differences among the electronic configurations $\Delta E$ as a function of $U_{\rm eff}$ for (a) $MnCp_2$ and (b) $CrCp_2$. The diamonds (blue) and triangles (red) in (a) represent the $^2E_{2g}$ and $^6A_{1g}$ states, respectively, and the diamonds (blue), triangles (red), and squares (green) in (b) represent the $^3E_{2g}$, $^3A_{1g}$, and $^5E_{1g}$ states, respectively. $U_{\rm eff} = 0$ eV corresponds to the GGA results.

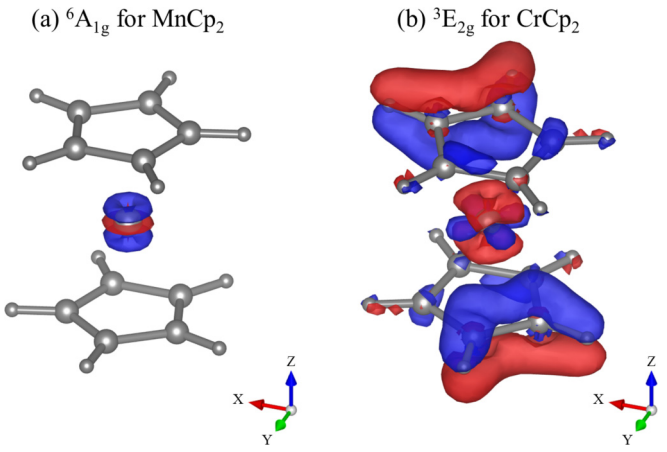


FIG. 5. Charge-density difference $\Delta\rho = \rho_{MCp_2} - (\rho_{Cp_2} + \rho_M)$ for (a) $^6A_{1g}$ $MnCp_2$ and (b) $^3E_{2g}$ $CrCp_2$ for GGA + $U$ with $U_{\rm eff}^{\rm LRT}$. The blue and red regions indicate positive (accumulation) and negative (depletion) differences, respectively.

$\Delta\rho = \rho_{MnCp_2} - (\rho_{Cp_2} + \rho_{Mn})$ of the $^6A_{1g}$ state shows small changes in the $d$ orbitals around the Mn site but almost no changes in the molecular orbitals in the ligand $Cp_2$.

For $CrCp_2$, the GGA calculations give stationary solutions for both $^3E_{2g}$ and $^3A_{1g}$ with the total energy of the $^3E_{2g}$ state lower than the $^3A_{1g}$ one by 0.32 eV as shown in Fig. 4(b). $\Delta E$ for the $^3A_{1g}$ state decreases as $U_{\rm eff}$ increases and becomes stable when $U_{\rm eff}$ is larger than about 4 eV. For $U_{\rm eff}^{\rm LRT}$ (=2.3 eV), the ground state is the $^3E_{2g}$ state, and the electronic configuration does not change due to electron correlation effects. As seen in Fig. 5(b), the charge-density difference has significant hybridization between the Cr $d_{x^2-y^2,xy}$ and the $Cp_2$ $e_{2g}$ orbitals. In this system, the single occupation of the doublet $d_{x^2-y^2,xy}$ causes a Jahn-Teller distortion that leads to the $^3E_{2g}$ ground state. In contrast, the $^3A_{1g}$ state predicted by previous $+U$ [19] and B3LYP [20] calculations corresponds to the metastable state in the present constraint DFT calculations.

Finally, for $VCp_2$, the ground state is predicted to be $^4A_{2g}$ in both GGA and GGA $+ U$, in agreement with experiments [15–18] and the previous calculations [19,20]. No other stationary solutions were found, even for large constraint fields. These results are not surprising since the singlet $d_{z^2}$ and the doublet $d_{x^2-y^2,xy}$ in the majority-spin states are fully occupied, which stabilizes the high-spin state.

## IV. SUMMARY

We have used constraint DFT calculations to search for the ground-state electronic configurations of correlated organometallic metallocenes including electron correlations via nonempirical $U_{\rm eff}$ determined from linear response. We find that the calculated ground states are sensitive to the $U_{\rm eff}$ values and to Jahn-Teller splittings. Our predicted ground states based on constraint DFT and linear-response-determined values of $U_{\rm eff}$ are found to be in agreement with the experiments; thus demonstrating the utility of constraint DFT searches to determine the properties of correlated systems.

## ACKNOWLEDGMENTS

We thank Professor T. Oguchi for fruitful discussions. Work at Mie University was supported by a Grant-in-Aid for JSPS Fellows Grant No. 16J07422 and Scientific Research Grant No. 16K05415 from the Japan Society for the Promotion of Science and the Cooperative Research Program of "Network Joint Research Center for Materials and Devices." Computations were performed at the Research Institute for Information Technology, Kyushu University and the Supercomputer Center, Institute for Solid State Physics, University of Tokyo. Work at UWM was supported by the National Science Foundation, Grant No. DMR-1335215.

[1] V. V. Maslyuk, A. Bagrets, V. Meded, A. Arnold, F. Evers, M. Brandbyge, T. Bredow, and I. Mertig, Phys. Rev. Lett. **97**, 097201 (2006).
[2] C. Morari, H. Allmaier, F. Beiuseanu, T. Jurcut, and L. Chioncel, Phys. Rev. B **85**, 085413 (2012).
[3] M. Wu and X. C. Zeng, Appl. Phys. Lett. **99**, 053121 (2011).
[4] Y. Li, Z. Zhou, and Z. Chem, J. Phys. Chem. A **116**, 1648 (2012).
[5] N. Hoshino, F. Iijima, G. N. Newton, N. Yoshida, T. Shiga, H. Nojiri, A. Nakao, R. Kumai, Y. Murakami, and H. Oshio, Nat. Chem. **4**, 921 (2012).
[6] B. Himmetoglu, A. Floris, S. de Gironcoli, and M. Cococcioni, Int. J. Quantum Chem. **114**, 14 (2014).
[7] B. Himmetoglu, A. Marchenko, I. Dabo, and M. Cococcioni, J. Chem. Phys. **137**, 154309 (2014).
[8] T. J. Kealy and P. L. Pauson, Nature (London) **168**, 1039 (1951).
[9] N. J. Long, *Metallocenes: An Introduction to Sandwich Complexes* (Blackwell Science, London, 1988).
[10] E. Wimmer, H. Krakauer, M. Weinert, and A. J. Freeman, Phys. Rev. B **24**, 864 (1981).
[11] M. Weinert, E. Wimmer, and A. J. Freeman, Phys. Rev. B **26**, 4571 (1982).
[12] A. B. Shick, A. I. Liechtenstein, and W. E. Pickett, Phys. Rev. B **60**, 10763 (1999).
[13] K. Nakamura, Y. Kitaoka, T. Akiyama, T. Ito, M. Weinert, and A. J. Freeman, Phys. Rev. B **85**, 235129 (2012).
[14] Y. Kitaoka, K. Nakamura, T. Akiyama, T. Ito, M. Weinert, and A. J. Freeman, Phys. Rev. B **87**, 205113 (2013).
[15] S. Evans, M. L. H. Green, B. Jewitt, A. F. Orchard, and C. F. Pygall, J. Chem. Soc., Faraday Trans. 2 **68**, 1847 (1972).
[16] S. Evans, M. L. H. Green, B. Jewitt, G. H. King, and A. F. Orchard, J. Chem. Soc., Faraday Trans. 2 **70**, 356 (1974).
[17] K. R. Gordon and K. D. Warren, Inorg. Chem. **17**, 987 (1978).
[18] M. F. Retting and R. S. Drago, J. Am. Chem. Soc. **91**, 1361 (1969).
[19] Y. Ma, Y. Dai, W. Wei, and B. Huang, J. Mater. Chem. C **1**, 941 (2013).
[20] Z. F. Xu, Y. M. Xie, W. L. Feng, and H. F. Schaefer, J. Phys. Chem. A **107**, 2716 (2003).
[21] J. P. Perdew, K. Burke, and M. Ernzerhof, Phys. Rev. Lett. **77**, 3865 (1996).
[22] M. Cococcioni and S. de Gironcoli, Phys. Rev. B **71**, 035105 (2005).
[23] I. Langmuir, Science **54**, 59 (1921).